Biochemistry

Article

Cite This: Biochemistry 2019, 58, 1275−1286

pubs.acs.org/biochemistry

Tracking Pore Hydration in Channelrhodopsin by Site-Directed Infrared-Active Azido Probes

Benjamin S. Krause,[†] Joel C. D. Kaufmann,[‡,§] Jens Kuhne,[∥] Johannes Vierock,[†] Thomas Huber,[⊥] Thomas P. Sakmar,[⊥,#] Klaus Gerwert,[∥] Franz J. Bartl,[‡,§] and Peter Hegemann*[,†]

[†]Institut für Biologie, Experimentelle Biophysik, Humboldt-Universität zu Berlin, Invalidenstrasse 42, 10115 Berlin, Germany

[‡]Institut für Biologie, Biophysikalische Chemie, Humboldt-Universität zu Berlin, Invalidenstrasse 42, 10115 Berlin, Germany

[§]Institut für medizinische Physik und Biophysik, Charité-Universitätsmedizin, Berlin, Charitéplatz 1, 10117 Berlin, Germany

[∥]Lehrstuhl für Biophysik, Ruhr-Universität Bochum, Universitätsstrasse 150, 44801 Bochum, Germany

[⊥]Laboratory of Chemical Biology & Signal Transduction, The Rockefeller University, 1230 York Avenue, New York, New York 10065, United States

[#]Department of Neurobiology, Care Sciences and Society, Division for Neurogeriatrics, Center for Alzheimer Research, Karolinska Institutet, Alfred Nobels Allé 23, 141 57 Huddinge, Sweden

Supporting Information

ABSTRACT: In recent years, gating and transient ion-pathway formation in the light-gated channelrhodopsins (ChRs) have been intensively studied. Despite these efforts, a profound understanding of the mechanistic details is still lacking. To track structural changes concomitant with the formation and subsequent collapse of the ion-conducting pore, we site-specifically introduced the artificial polarity-sensing probe *p*-azido-L-phenylalanine (azF) into several ChRs by amber stop codon suppression. The frequently used optogenetic actuator ReaChR (red-activatable ChR) exhibited the best expression properties of the wild type and the azF mutants. By exploiting the unique infrared spectral absorption of azF [$\nu_{as}(N_3) \sim 2100\ cm^{-1}$] and its sensitivity to polarity changes, we monitored hydration changes at various sites of the pore region and the inner gate by stationary and time-resolved infrared spectroscopy. Our data imply that channel closure coincides with a dehydration event occurring between the interface of the central and the inner gate. In contrast, the extracellular ion pathway seems to be hydrated in the open and closed states to similar extents. Mutagenesis of sites in the inner gate suggests that it acts as an intracellular entry funnel, whose architecture and composition modulate water influx and efflux within the channel pore. Our results highlight the potential of genetic code expansion technology combined with biophysical methods to investigate channel gating, particularly hydration dynamics at specific sites, with a so far unprecedented spatial resolution.

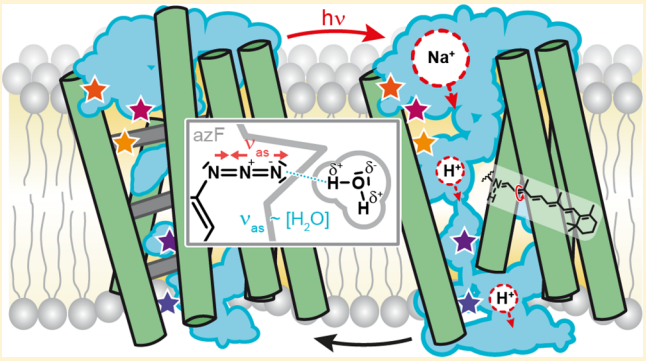

Channelrhodopsins (ChRs) are light-gated ion channels that conduct protons,[1,2] cations,[3,4] or anions.[5,6] Their seven-transmembrane helix (H) bundle accommodates a retinal chromophore covalently linked via a retinal Schiff base (RSB) to a highly conserved lysine residue (Figure 1A). In 2012, Kato et al. determined the crystal structure of the dark state of the cation-conducting ChR chimera C1C2 composed of ChR1 (H1−H5) and ChR2 (H6 and H7) of *Chlamydomonas reinhardtii* and revealed the first detailed structural information regarding the ion channel architecture (Figure 1A).[7] The putative channel pore is formed by residues of H1−H3 and H7, including several negatively charged glutamates in H2, and becomes wider at the extracellular side (half-channel). In the dark, the pore is blocked by two spatial constrictions. One is situated in the core of the photoreceptor close to the RSB, called the central gate (S102, E129, and N297 in C1C2), and the other faces the intracellular side, termed the inner gate (Y109, E121, E122, H173, H304, and R307 in C1C2). Computational calculations predicted a discontinuous water distribution within the transport path for the dark state of ChRs due to the channel gate(s).[8−12] Upon photoactivation, ChRs undergo global helix movements of H2 and H7[9,10,13,14] and/or partial unwinding of the cytoplasmic end of H2,[15] which is expected to constitute the conductive state. However, the detailed molecular mechanism of channel opening and closing in ChRs, especially formation and decay of a hydrated pore, is barely understood.

Received: November 22, 2018
Revised: January 31, 2019
Published: January 31, 2019

DOI: 10.1021/acs.biochem.8b01211
Biochemistry 2019, 58, 1275−1286

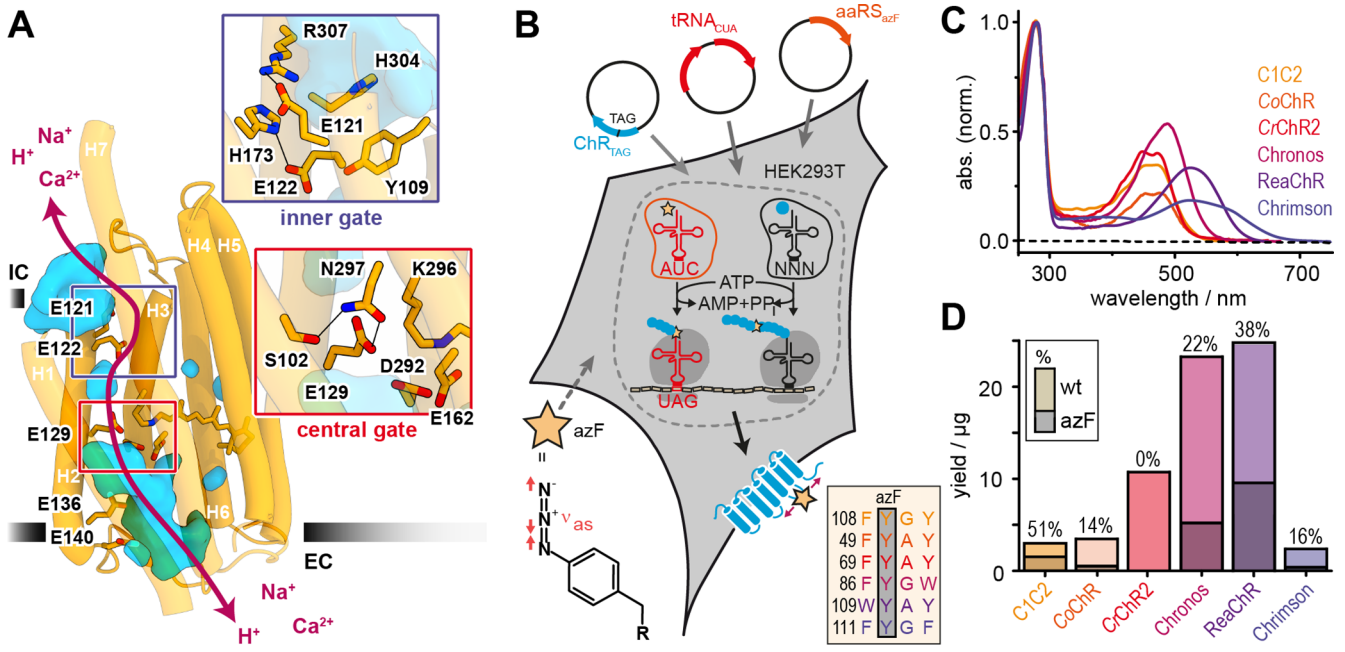

Figure 1. Introduction of IR-active *p*-azido-L-phenylalanine (azF) into channelrhodopsins. (A) Structural overview of the putative ion-conducting pathway (magenta arrow) of the channelrhodopsin C1C2 (Protein Data Bank entry 3ug9) flanked by helix 2 glutamates that is interrupted in the dark by the interhelical hydrogen bond networks of the inner gate (blue) and the central gate (red). Helices are marked as H1−H7 and cavities within the protein (faint blue) were predicted by HOLLOW. (B) Simplified scheme of stop codon suppression. HEK293T cells are co-transfected with three plasmids encoding the amber mutant of ChR (ChR_{TAG}), the suppressor tRNA with a complementary anticodon ($tRNA_{CUA}$), and the evolved aminoacyl tRNA synthetase ($aaRS_{azF}$). $tRNA_{CUA}$ is charged by $aaRS_{azF}$ with the unnatural substrate azF (yellow star), which is integrated into the nascent polypeptide chain built by canonical amino acids (blue circles) in response to a TAG codon on the mRNA. The target site is highlighted in the sequence alignment (gray box). (C) Normalized UV−vis spectra of purified ChRs in Dulbecco's phosphate-buffered saline (DPBS) (pH 7.4) with 0.03% (w/v) *n*-dodecyl *β*-D-maltopyranoside (DDM). (D) Yields (in micrograms per 100 mm culture dish) of recombinant wild types (plain bars, expression for 36−48 h) and corresponding azF mutants (shaded bars, expression for 76−86 h). The suppression efficiency (yield of azF mutant/yield of wild type) is listed above each column.

To investigate the molecular details of reaction mechanisms of photoreceptors, Fourier transform infrared (FTIR) difference spectroscopy is a powerful tool and over the past several decades has been successfully applied to elucidate light-induced reaction pathways of microbial and vertebrate rhodopsins.[16−18] It allows one to monitor minute alterations in specific receptor groups, involving proton transfer reactions, changes in hydrogen bonding, secondary structural changes, and chromophore movements. Time-resolved FTIR techniques provide profound insight into the photocycle dynamics in the time range from nanoseconds (step scan) to seconds (rapid scan).[19] For the assignment of bands in the FTIR difference spectra, a number of methods such as site-directed mutagenesis and ^{13}C labeling were developed.[20] Changes in the secondary structure are usually derived from the amide I (1700−1620 cm^{-1}) and amide II (1570−1510 cm^{-1}) bands of the protein backbone. However, they report simultaneously on a multitude of structural moieties of the entire protein, so that a clear assignment to distinct protein regions is complicated and requires more sophisticated labeling techniques for a site-specific assignment.

Global isotopic labeling of a group of residues by selective pressure incorporation (SPI)[21,22] or stable isotopic labeling of amino acids in cell culture (SILAC)[23−26] is a nonperturbative method and allows a better assignment of certain bands. However, replacement by SPI and SILAC is solely advantageous for IR studies when the residues chosen for substitution occur in small quantities, preferentially as a single copy. Moreover, incorporation of isotopically labeled cofactors can assist in the identification of chromophore bands.[27]

Artificial IR reporters like azido (N_3),[28−30] cyano (CN),[28,31−33] and thiocyanato (SCN)[28,34,35] are beneficial for vibrational spectroscopy in several respects. First, they provide specific information about single-residue dynamics within their protein microenvironments. Second, they are relatively strong chromophores ($\varepsilon \sim 250-680$ M^{-1} cm^{-1})[28,36,37] and absorb in a spectral window lacking endogenous protein vibrations (2300−2050 cm^{-1}). Lastly, they are sensitive to subtle changes in their electrostatic environment (vibrational Stark effect),[38] particularly caused by alterations of their hydration status due to hydrogen bonding interactions.[39,40]

In contrast to early approaches to incorporating IR reporter groups by chemical peptide synthesis,[28,31] which is rather limited to smaller polypeptides, these probes can be integrated into proteins either co-translationally as methionine analogues (azido homoalanine and azido norleucine)[41−43] or post-translationally by cysteine alkylation[33] or cyanylation (SCN).[34] As ChRs contain several copies of (functional) methionine (≥7) and cysteine residues (≥6), global replacement would result in a complex, superimposed spectrum of several reporters. To decrease the number of target sites, intensive mutant screening (and subsequent characterization) is mandatory. Additionally, chemical downstream transformation of cysteines is virtually limited to accessible, solvent-exposed labeling sites. More importantly, some cysteines are functionally relevant and/or crucial for

DOI: 10.1021/acs.biochem.8b01211
Biochemistry 2019, 58, 1275−1286

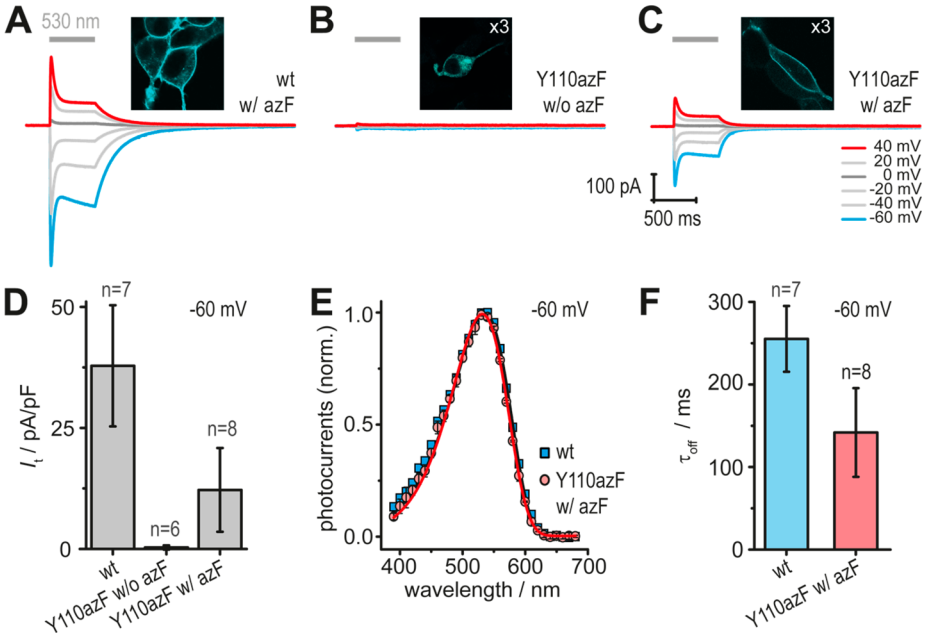

Figure 2. Electrophysiological and microscopic performance analysis of the orthogonal pair. Whole cell patch clamp recordings and laser scanning confocal microscopy of HEK293T cells expressing ReaChR in the presence of (A) azF and the azido mutant Y110azF (C) with or (B) without azF in the medium. HEK293T cells were co-transfected with plasmids encoding $tRNA_{CUA}$ and $aaRS_{azF}$. For confocal images, mCerulean3 fluorophores were excited with 2 and 6% laser power for the wild type (A, inset) and Y110azF (B and C, insets), respectively. The appearance of any fluorescence in the Y110azF experiment lacking azF speaks to a truncated and/or poorly folded product potentially based on a translation restart via a methionine downstream from the amber codon. (D) Peak photocurrents (I_t) of panels A−C plotted as a bar diagram. (E) Normalized action spectra (10 ms activation) of the wild type (blue squares) and Y110azF (red circles). Data points were fitted with Weibull functions. (F) Channel closure kinetics (apparent τ_{off}, biexponential fit) of the wild type (blue) and Y110azF (red) upon green illumination (530 nm, 500 ms). Data in panels D−F represent means ± the standard deviation.

protein stability and integrity, so that mutagenesis could cause a complete lack of expression.[44]

Alternatively, the site-directed integration of IR sensors can be achieved in a one-step procedure using genetic code expansion by stop codon suppression. Site-directed mutagenesis is utilized to place one of the three stop codons (TAG, amber) inside the gene of interest, which is then recognized by a modified suppressor tRNA with a complementary anticodon. The suppressor tRNA is charged *in vivo* with the IR-active unnatural amino acid by an evolved aminoacyl tRNA synthetase (aaRS). Most of the published orthogonal pairs (suppressor tRNA and aaRS) are primarily functional in *Escherichia coli*, but expression of eukaryotic membrane proteins like ChRs is not trivial in the lower prokaryote.[45−48] Therefore, we previously designed an orthogonal pair ($tRNA_{CUA}$ and $aaRS_{azF}$) for incorporating *p*-azido-L-phenylalanine (azF) into proteins expressed in human embryonic kidney (HEK293T) cells (Figure 1B). For example, this system was applied for the selective incorporation of azF into bovine rhodopsin (bR).[29,30]

In the study presented here, we employed genetic code expansion in different ChRs using amber stop codon suppression. We achieved optimal yields of labeled protein for the well-characterized red light-activatable ChR (ReaChR).[49] Site-specific labeling with azF at different positions along the putative channel pore allowed the localization of changes in protein hydration by steady-state and time-resolved FTIR spectroscopy at molecular resolution. Our data imply that channel closing is associated with a late dehydration event within the interface of the inner and central gate and that the inner gate modulates the migration of water into this compartment. These findings complement our previous studies of green-absorbing ReaChR[50,51] and are relevant for the application of this frequently used optogenetic tool[49,52] and furthermore pave the way for a more general understanding of pore formation and collapse in ChRs.

RESULTS

Expression of ChRs and Azido Mutants in HEK293T Cells. To incorporate the unnatural IR-active amino acid *p*-azido-L-phenylalanine (azF) into ChRs, we assessed expression levels of six different wild-type proteins in HEK293T cells. Maximal expression was observed ∼36 h after transfection (Figure S1, left). Purified photoreceptors were investigated by ultraviolet−visible (UV−vis) spectroscopy (Figure 1C), and yields were determined from chromophore absorption (Figure 1D, plain bars). Chronos, a ChR from *Stigeoclonium helveticum*,[53] and ReaChR[49] exhibited the highest level of expression (>20 μg/dish). As Y109 in C1C2 (H1) is part of the inner gate blocking the putative ion channel pathway toward the cytoplasmic side in the closed state,[7,54] it was chosen as a target site to probe local dynamics upon photoactivation and channel opening as well as channel closure. Additionally, tyrosine substitution against azF results in a sterically similar side chain and is thus less invasive. Therefore, Y109 in C1C2 and the homologous tyrosines in the other ChRs (Figure 1B, bottom right) were replaced by azF using amber stop codon suppression (Figure 1B). Expression maxima of the azF mutants were delayed compared with those of wild-type proteins and peaked roughly 83 h after transfection (Figure S1, right). Yields of purified mutants are depicted in Figure 1D (shaded bars). Even though C1C2

DOI: 10.1021/acs.biochem.8b01211
Biochemistry 2019, 58, 1275−1286

possessed the highest suppression efficiency (yield of azF mutant/yield of wild type), amber mutants of Chronos (Y87azF) and ReaChR (Y110azF) showed the largest absolute protein amounts. Given the superior expression properties of ReaChR, we proceeded with the green-absorbing chimera for subsequent experiments.

Performance Analysis of the Orthogonal Pair by Microscopy and Electrophysiology. To test whether the applied orthogonal pair of suppressor $tRNA_{CUA}$ and $aaRS_{azF}$ specifically recognizes azF and whether the functionality of the expressed azF mutant is preserved in the presence of the artificial analogue, electrical measurements under voltage clamp conditions were performed for ReaChR and Y110azF. All HEK293T cells used for electrophysiological measurements and confocal microscopy were co-transfected with $tRNA_{CUA}$ and $aaRS_{azF}$. Current traces of the wild type with azF supplemented in the medium (Figure 2A) resemble currents of the wild type without the addition of azF,[50] while the peak current amplitude is reduced 3-fold in the amber mutant (Figure 2C,D), most likely due to the reduced level of expression of full-length protein. This is consistent with a weaker fluorescence signal of the amber mutant seen in confocal images (Figure 2C, inset). Strikingly, light-induced currents of Y110azF in the absence of azF are hardly detectable (Figure 2B,D), indicating a small quantity of unspecific read-through of the UAG codon and accumulation of the truncated product that does not drive ion transport. Incorporation of azF does not affect the λ_{max} of the action spectrum reporting for wavelength-dependent photocurrents (Figure 2E), but channel closure kinetics of Y110azF after illumination (530 nm, 500 ms) are slightly faster than in the wild-type protein (Figure 2F).

Bioorthogonal Coupling of ReaChR with Incorporated azF to Fluorophores. To verify functional incorporation and conservation of azF in ReaChR, the two azF mutants Y112azF and W115azF (H1; cf. Figure 4A) and the wild type (without incorporated azF) were coupled to a dibenzyl cyclooctyne (DIBO)-conjugated fluorophore (Alexa647) via strain-promoted alkyne–azide cycloaddition [SPAAC (Figure 3A)]. The coupling efficiency was determined by in-gel fluorescence (inset) and UV–vis spectroscopy (Figure 3B). As expected, the wild type yielded a poor signal in the fluorescence scan but a background labeling of 0.16. This relatively high extent of unspecific binding could be explained by accidental cross-reaction to exposed thiol side chains[55] (Figure S7). In contrast to the wild type, Y112azF and W115azF showed strong fluorescence and labeling stoichiometries, $(A_{Alexa}/\varepsilon_{Alexa})/(A_{ChR}/\varepsilon_{ChR})$, of 0.84 and 0.55, respectively. The nonquantitative labeling was attributed to either the restricted accessibility of both sites shielded by the lipidic bilayer (Figure S5i) or the different hydrophobicity of the label environment affecting reaction kinetics.[56] Furthermore, adjacent mercapto groups could inactivate azides by reduction,[57] thereby decreasing the absolute content of functional N_3 handles. Nevertheless, at least 70% of azF (for Y112azF) is efficiently incorporated into ReaChR in its IR-active form without significant decomposition of the azido moiety during the purification and labeling procedure.

Steady-State Fourier Transform Infrared Spectroscopy. To identify suitable sites reporting on polarity changes concomitant with channel gating, we introduced azF at eight different positions within the putative channel pore (K133, F142, and Y283), the inner gate (Y110 and N305), the C-terminal end of H1 (Y112 and W115), and intracellular loop 1 (ICL1, C119) (colored stars, Figure 4A). While the yields of recombinant azF mutants strongly depend on the individual target site at which the unnatural amino acid was integrated (Figure 4B), absorption maxima were largely unaffected (Figure 4C). Next, we performed FTIR (light minus dark) difference spectroscopy of the well-expressing mutants and the wild type under photostationary conditions [~530 nm light-emitting diode (LED) excitation]. The spectra of the mutants resemble the wild-type spectrum but show alterations in the carboxylic region (Figure S2A,B) and altered intensities of amide I bands (Figure 4D, right).

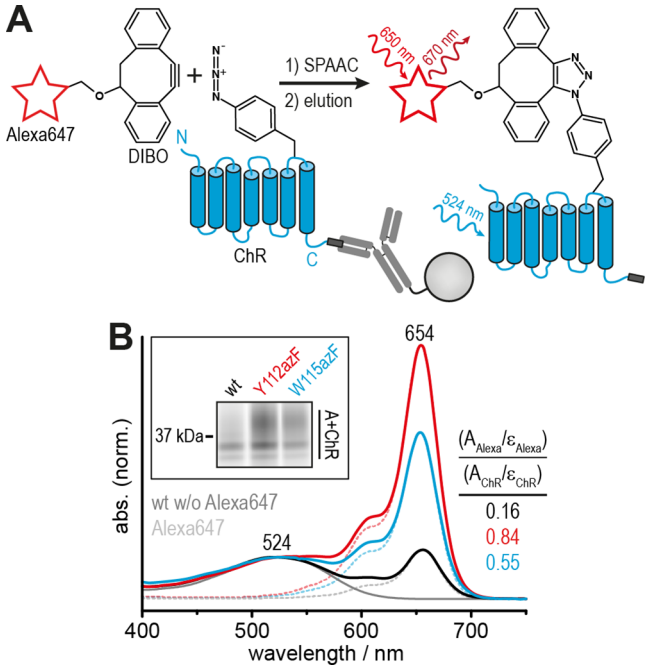

Figure 3. Bioorthogonal labeling of azF mutants with a red cyanine fluorophore. (A) Coupling of incorporated azF with a dibenzyl cyclooctyne (DIBO)–Alexa647 conjugate via strain-promoted alkyne–azide cycloaddition (SPAAC). (B) Normalized UV–vis spectra of ReaChR wild type (black solid line), Y112azF (red solid line), and W115azF (blue solid line) after hybridization to Alexa647. Spectra of the untreated wild type (gray solid line) and fractions of coupled Alexa dye are shown (colored dotted lines). The coupling efficiencies are listed. A fluorescence scan of the polyacrylamide gel after electrophoresis of 100 ng of labeled protein is depicted in the inset. M_w(ReaChR) = 39.6 kDa; M_w(Alexa647–DIBO) ~ 1.5 kDa.

In contrast to the wild type, Y110azF, K133azF, and F142azF show a complex band pattern in the high-frequency window around 2100 cm^{-1} [$\nu_{as}(N_3)$] that differs in shape and amplitude (Figure 4D, left). Strikingly, the Y110azF difference spectrum reveals two positive bands at 2119 and 2089 cm^{-1} and a negative one at 2108 cm^{-1} (Figure 4D, inset, apricot). In accordance with the solvatochromic frequency shift of free azF (Figure S3A), this indicates that a fraction of the Y110azF label experiences an increase (2119 cm^{-1}) and the other a decrease (2089 cm^{-1}) in the polarity of its environment upon illumination. The upshift from 2108(−) to 2119(+) cm^{-1} is similar to that of azF dissolved in water and isopropanol (Figure S3B,C) and leads to a reduced signal cancellation in the difference spectrum, which additionally contributes to the large amplitude of the band at 2119(+) cm^{-1}. The existence of two positive vibrations instead of a single band may result from

DOI: 10.1021/acs.biochem.8b01211
Biochemistry 2019, 58, 1275–1286

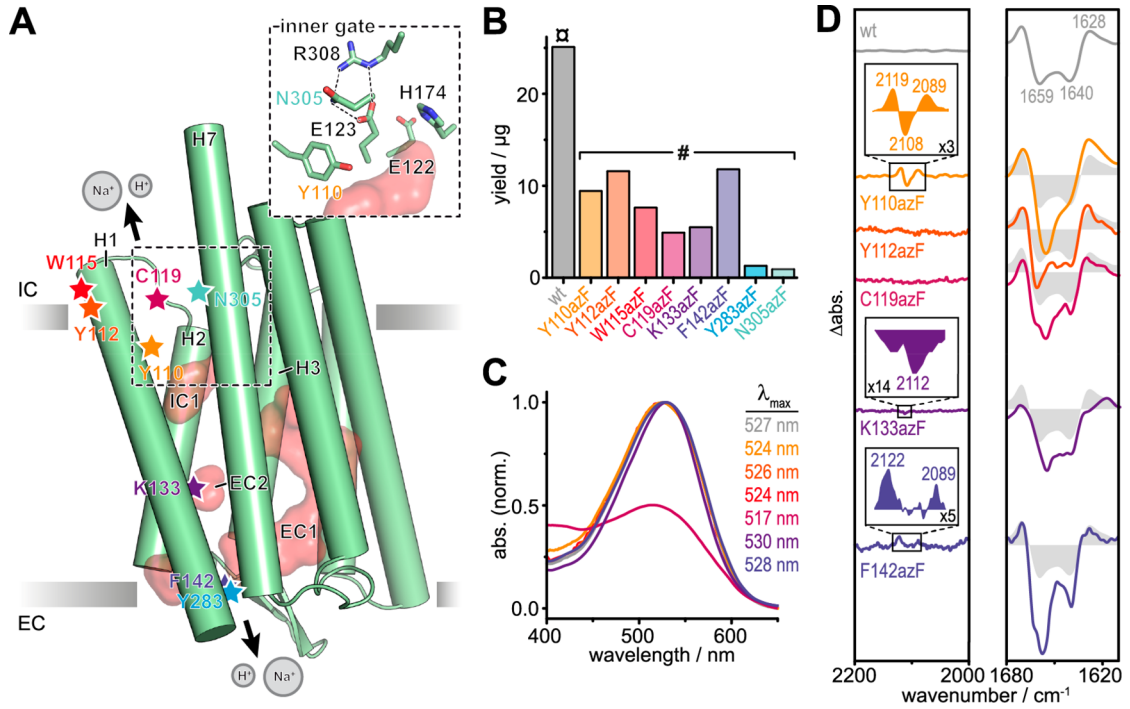

Figure 4. Incorporation of azF into ReaChR. (A) Structural model of ReaChR wild type created by Robetta. The membrane topology was estimated by the PPM server, and voids within membranous space (faint red) were predicted by HOLLOW. Target sites for azF (colored stars) within the putative ion pore (H1−H3 and H7, black arrows) are indicated. Residues of the inner gate are shown (inset, C119 not shown). Putative interactions (d < 3.5 Å) are indicated (dashed black lines). (B) Yields of ReaChR (100 mm culture dish, expression for 36 h, ¤) and azF mutants (expression for 76−86 h, #). (C) Normalized UV−vis spectra of recombinant proteins in DPBS (pH 7.4) with 0.03% (w/v) DDM at 20 °C. C119azF is unstable, like C79 mutants in *Cr*ChR2,[44] and shows free retinal ($\lambda \sim 400$ nm) and aggregation during purification. The spectrum was corrected for light scattering ($\sim\lambda^{-4}$) and scaled arbitrarily to 0.5. (D) Steady-state Fourier transform infrared (FTIR) (light minus dark) difference spectra of the wild type and azF mutants in DPBS (pH 7.4) with 0.03% (w/v) DDM upon illumination (~530 nm LED) representing the high-frequency (left) and amide I (right) windows. Enlarged difference spectra are shown (left, insets). The spectrum of the wild type is indicated (right, gray area). FTIR spectra are normalized to the retinal fingerprint band at 1200(−) cm^{-1} (cf. Figure S2A).

multiple substates with different label orientations coexisting under photostationary conditions. The possibility that the fine-structured signal is an intrinsic feature of the azido group due to accidental Fermi resonance[37,58,59] or superposition of symmetric and asymmetric oscillations[60] could also not be ruled out.

K133azF (purple) shows only one small negative band at 2112 cm^{-1}, and F142azF (violet) two positive ones at 2122 and 2089 cm^{-1} (Figure 4D). Because of the smaller signal amplitudes of both mutants compared with that of Y110azF, we conclude that light activation causes only minor polarity changes at these positions. The major light-induced band in F142azF [2122(+) cm^{-1}] is shifted by 3 cm^{-1} toward higher frequencies as compared with that of Y110azF, implying a slightly more polar environment of F142 in the illuminated state. Interestingly, the pronounced azF signals of Y110azF and F142azF are linked to enlarged amide I signals of the mutants in comparison with the wild type (Figure 4D).

No azido signal(s) was detected in the difference spectra of Y112azF (coral) or C119azF (pink) (Figure 4D), indicating only negligible polarity changes happening at the C-terminal end of H1 and ICL1 upon photoactivation. Consequently, the underlying vibrational bands of the dark state and the illuminated state largely cancel out each other in the difference spectrum.

Rapid-Scan Fourier Transform Infrared Spectroscopy. To assign local polarity changes to specific photocycle intermediates involving channel formation, Y110azF, K133azF, and F142azF were investigated by time-resolved FTIR spectroscopy (rapid scan, 532 nm laser excitation). As for the steady-state FTIR measurements, wild-type and Y110azF rapid-scan spectra are similar but show differences in the region indicative for ν(C═O) vibrations of carboxylic acid side chains (Figure S2C,D). The amplitude spectra of ReaChR (gray) and Y110azF (apricot) decayed with $t_{1/2}$ values of 300 and 320 ms, respectively. Thus, conformational changes reflected by the spectra are most likely correlated with channel closing [τ_{off}(wt) = 260 ± 40 ms (cf. Figure 2F)]. Besides an additional band at 2079(−) cm^{-1} in the amplitude spectrum of Y110azF, the band shape and peak position of $\nu_{as}(N_3)$ are virtually identical under single-turnover (Figure 5A, left, apricot) and photostationary (cf. Figure 4D, left, apricot) conditions as well as the increase in the amide I difference band compared with the wild-type band (Figure 5A, right, apricot). This might indicate different coexisting conformational substates of the Y110azF label as previously observed for the photostationary spectra (cf. Figure 4D), albeit less distinct because the time-resolved spectra reflect the formation of pure intermediates rather than a mixture of substates.

Alternatively, the band at 2090(+) cm^{-1} could be the upshifted counterpart to the negative band at 2079 cm^{-1}. Following this argument, conformational substates would be present already in the dark that both experience a relative polarity increase after illumination. In either of the two scenarios, the higher intensity of the band at 2119 cm^{-1}

DOI: 10.1021/acs.biochem.8b01211
Biochemistry 2019, 58, 1275−1286

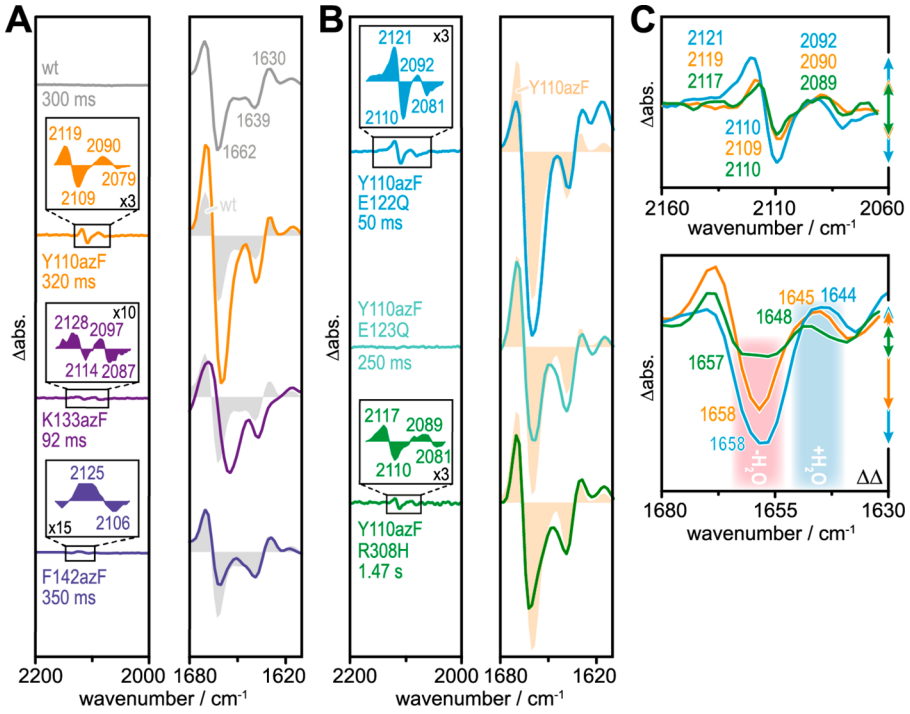

Figure 5. Time-resolved FTIR spectra of ReaChR and azF mutants. Rapid-scan FTIR amplitude spectra upon laser excitation (532 nm, 3−5 ns, 20 mJ, 0.4 Hz) in low-salt phosphate buffer (pH 7.4) with 0.03% (w/v) DDM of (A) azF single mutants and (B) three conventional inner gate mutants with the Y110azF backbone. Half-life times of decay ($t_{1/2}$) were obtained by global analysis. The high-frequency (left) and amide I (right) windows are shown. FTIR spectra are normalized to the retinal fingerprint band at 1200(−) cm^{-1} (cf. Figures S2C and S4B). (C) Overlay of azido difference spectra (top) and double-difference spectra (ΔΔ, $\Delta abs_{azF} - \Delta abs_{wt}$) of the amide I window (bottom) from panels A and B.

suggests a net polarity increase at the Y110azF label during the light reaction.

In contrast to the spectrum recorded under photostationary conditions, the difference spectrum of K133azF that decays with a $\mathbf{t}_{1/2}$ of 92 ms and was obtained under single-turnover conditions exhibits a higher complexity of the azido stretch vibration with two positive (2128 and 2097 cm^{-1}) and two negative bands (2114 and 2087 cm^{-1}) (Figure 5A, left, purple) due to accumulation of different photointermediates depending on the illumination conditions. In comparison with the difference spectrum of Y110azF, the high-frequency band pair [2128(+) and 2114(−) cm^{-1}] is blue-shifted by 5−9 cm^{-1}. This frequency upshift could point to a more polar milieu due to hydrogen bonding interactions within the active site (cf. Figure S2E). F142azF shows a band at 2125(+) cm^{-1} and a minor one at 2106(−) cm^{-1} (Figure 5A, left, violet), implying a polarity of the azF environment in the illuminated state between Y110azF [2119(+) cm^{-1}] and K133azF [2128(+) cm^{-1}].

To study the role of certain inner gate residues in the gating process, we combined Y110azF with conventional amino acid substitutions [E122Q, E123Q, and R308H/N (cf. Figure 4A, inset)]. Yields of generated double mutants Y110azF-E122Q, Y110azF-E123Q, and Y110azF-R308H were in the range of 34−44% of that of Y110azF (Y110azF-R308N did not show any chromophore binding), and the corresponding absorption spectra were only slightly shifted (Figure S4A). Y110azF-E122Q reveals a complex IR pattern with two positive (2121 and 2092 cm^{-1}) and two negative (2110 and 2081 cm^{-1}) bands in the azido region (Figure 5B, left, blue) that are upshifted by 1−2 cm^{-1} as compared with those of Y110azF. Moreover, the signal amplitude of $\nu_{as}(N_3)$ in the double mutant is enlarged, and the decay of the spectral species accelerated 6-fold ($t_{1/2}$ = 50 ms). Remarkably, Y110azF-E123Q lacks any high-frequency bands around 2100 cm^{-1} (Figure 5B, left, turquoise), although no significant alterations were observed in the <1800 cm^{-1} spectral window with respect to Y110azF (Figure S4B,C) and the kinetics were not affected ($t_{1/2}$ = 250 ms). Y110azF-R308H resulted in a frequency downshift of the positive bands by 1−2 cm^{-1} (2117 and 2089 cm^{-1}), while the dark-state bands are blue-shifted by 1−2 cm^{-1} [2110(−) and 2081(−) cm^{-1}] (Figure 5B, left, green). The signal amplitude of Y110azF-R308H is slightly reduced, and the decay kinetics is 4.5 times slower ($t_{1/2}$ = 1.47 s) than for the azF single mutant. On the basis of the spectral correlation between $\nu_{as}(N_3)$ and the polarity of the environment (cf. Figure S3) and the different signal amplitudes, E122Q causes larger and R308H smaller polarity changes compared with that of the parental Y110azF mutant (Figure 5C, top). This finding correlates with the amplitude of the corresponding amide I oscillations that are enhanced in Y110azF-E122Q and reduced in Y110azF-R308H (Figure 5B), a trend that is even more clearly seen in the double-difference spectra in which a pair of bands [1658/57(−) and 1648−44(+) cm^{-1}] is detected (cf. Figure 5C, bottom). Like for *Cr*ChR2,[61] the frequency downshift of these bands could be caused by hydrogen bonding of backbone carbonyls to adjacent water molecules. Accordingly, we assign the band pair to C═O oscillations of dehydrated and hydrated α-helices.

DISCUSSION

Unnatural Amino Acid Mutagenesis within Channelrhodopsins. As demonstrated here, incorporated unnatural amino acids like azF can be selectively derivatized or

DOI: 10.1021/acs.biochem.8b01211
Biochemistry 2019, 58, 1275−1286

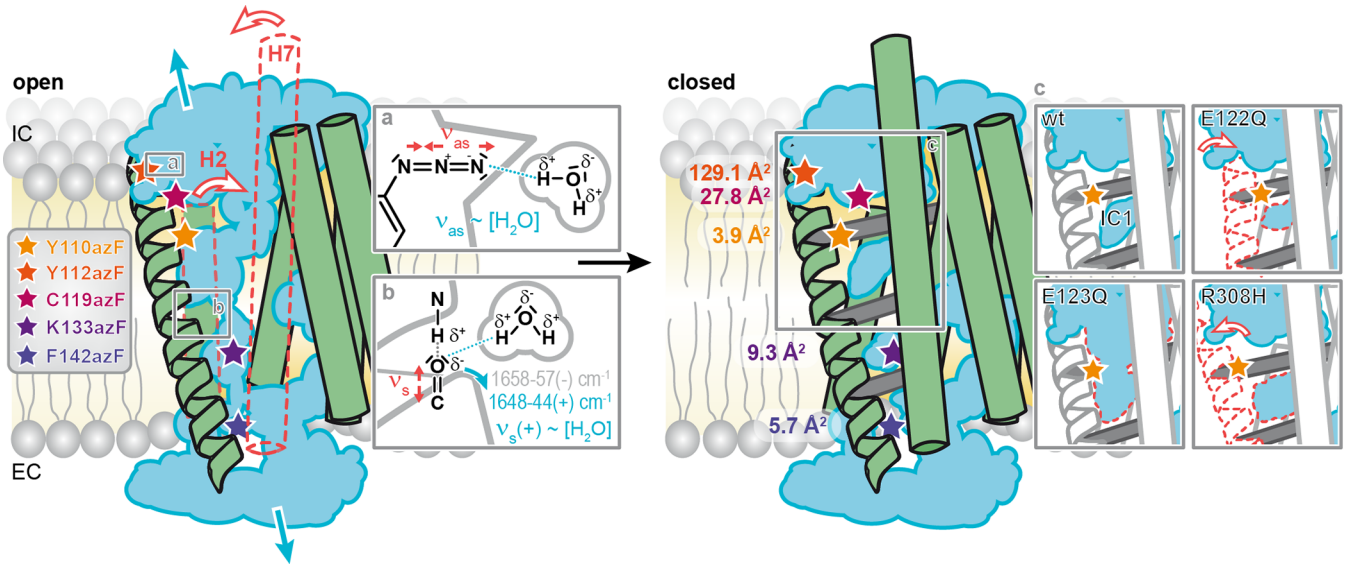

Figure 6. Hydration of the channel pore in ReaChR. Upon channel closure, H2 and H7 (red dashed cylinders) reorient[9,10,13−15] and the aqueous pore collapses followed by re-formation of the structural gates (gray bars). General interactions of water with (a) azF and (b) backbone carbonyls are illustrated (insets). Solvent accessible surface areas (SASA, in square angstroms) of the native amino acids in the Robetta dark-state structure were calculated by GETAREA (right). (c) Influence of inner gate mutants on the hydration level in the dark state. The E122Q mutation leads to a smaller water population and R308H to a larger water population in the dark state (red dashed area) compared with that of the wild type. In E123Q, the inner gate becomes leaky, i.e., early (non-light-induced) water penetration of the gate interface.

transformed into nonproteinogenic functionalities and/or used as highly selective infrared labels reporting on local polarity changes inside the protein. Besides application as an infrared label, azF was exploited as a chemical handle for bioorthogonal coupling to fluorophores[62,63] or epitopes[64] and for photo-cross-linking.[65−68] Our orthogonal pair for azF has already been successfully applied to investigate the function of G protein-coupled receptors,[29,30,64,66] ionotropic receptors,[67,69] and a neurotransmitter transporter.[68] In the study presented here, we applied this technique to light-gated ion channels, channelrhodopsins, and demonstrated the substrate specificity for azF by electrophysiological recordings (cf. Figure 2). The incorporation efficiency, though, strongly depends on the individual ChR variant and the selected target site, as previously reported for bovine rhodopsin.[29] Among the six tested ChR constructs, ReaChR, a frequently used optogenetic actuator,[49,52] showed superior expression (cf. Figure 1D), functional integration, and preservation of the azido moiety in recombinant form (cf. Figure 3). Strikingly, our *in vivo* labeling strategy succeeded even for non-solvent-exposed, embedded positions inside the protein core [K133 (cf. Figure 4A)], a task that is not easily achieved *in vitro* for the recombinant protein in the folded state. The FTIR (light minus dark) difference spectra of ReaChR azF mutants revealed a series of complex band patterns in the high-frequency window around 2100 cm^{-1} indicative of the (asymmetric) stretch vibrations of the unsaturated homoatomic nitrogen bonds [$\nu_{as}(N_3)$ (cf. Figures 4D and 5A,B)]. The signal complexity could be mainly attributed to coexisting photocycle states with different side chain rotamers and/or Fermi resonance of the azido group.[37,58,59] Free azF (cf. Figure S3) and other azido-containing model compounds show spectral shifts when dissolved in different (a)protic solvents (solvatochromic effect),[28,40] thus reporting on polarity changes of their environments. In the context of a protein, these polarity changes could arise from local electrostatic field changes or local water solvation around the labeling site or from global conformational changes inducing new nonsolvent H-bonding interactions with the label. Boxer and colleagues reported a low sensitivity of the vibrational frequency of azido bands to electric fields.[36,60] Given that, electrostatics are expected to have a minor impact on the azF frequency and either local water dynamics or the formation of secondary H-bonds seems to be more important. As azF was incorporated within the putative ion pore, which is expected to become at least partially hydrated upon photoactivation, light-induced polarity changes should result mainly from (de)hydration events occurring within the azF microenvironment.

Pore Hydration in Channelrhodopsin. In the closed configuration of ChRs, passive ion transport across the membrane is inhibited by at least two spatial constrictions within the putative ion pathway, i.e., inner and central gate (as in C1C2),[7,54] and an additional outer or extracellular gate (as in Chrimson and *Cr*ChR2).[70,71] Accordingly, water molecules along the channel pore are not continuously distributed[8−12] but rather concentrated in patches within interior cavities (cf. Figure S5). Upon illumination, structural rearrangements change the water distribution inside the pore and allow proton and cation conductance throughout the hydrophobic lipid bilayer. A glutamate in the central gate was identified to be part of the selectivity filter promoting transport of protons over monovalent cations.[51,72] On the basis of steered molecular dynamics simulations, the trajectory of sodium transport was proposed to be alongside the putative ion pore built by H1−H3 and H7, where Na^+ enters via the extracellular half-channel, passes the central gate, and exits between H2, H3, and H7 and ICL1.[73] A series of spectroscopic, microscopic, and computational studies of *Cr*ChR2 and C1C2 have identified light-induced helix movements of H2 and H7[9,13−15] and suggested a sequential gating process.[10,61]

Because of the limited time resolution of the rapid-scan measurements (≥6 ms after excitation), we were not able to

DOI: 10.1021/acs.biochem.8b01211
Biochemistry 2019, 58, 1275−1286

monitor early conformational and hydration changes associated with (pre)gating and/or channel opening. However, the temporal correlation between the decay of the time-resolved FTIR spectra of ReaChR [$t_{1/2} \sim 300$ ms (cf. Figure 5A)] and the cessation of ion conductance within electrophysiological recordings [$\tau_{off} = 260 \pm 40$ ms (cf. Figure 2F)] indicates that the spectral changes reflect channel closing. As the FTIR data could be properly described by a single time constant, closure of the ion pore is expected to be achieved in one concerted structural action. This is in accordance with the case for *Cr*ChR2, for which time-resolved FTIR and electrophysiological measurements have suggested that channel closing parallels partial water efflux toward the intracellular side.[61] While the aforementioned interpretation mainly relies on the rather unspecific amide I oscillations, an assignment to distinct regions within the protein was not possible. In this respect, our approach provides a clear advantage because site-specific polarity-sensitive IR labels allowed us to track polarity changes and thus (de)hydration events within different protein compartments. Because major water motions are expected to occur within the putative ion pathway, we introduced azF into the different channel sections, including intracellular loop 1, inner gate, extended active site, and extracellular half channel (cf. Figure 4A).

As expected for target sites within the C-terminal end of H1 and ICL1 in ReaChR (Y112azF and C119azF), no polarity changes were monitored (cf. Figure 4D), because both Y112 and C119 probably face the extracellular bulk already in the dark state (cf. Figure S5D). A water-exposed orientation of both residues in the closed configuration is indicated by their large solvent accessible surface areas (SASA; 129.1 Å^2 for Y112 and 27.8 Å^2 for C119) in the three-dimensional models (Figure 6). C119 corresponds to C79 in *Cr*ChR2, which was used for site-directed spin and fluorophore labeling before. The electron parametric resonance and fluorescence measurements of C79-labeled *Cr*ChR2 revealed a light-triggered (outward) movement of the N-terminal end of H2,[13,14,74] which might be reverted during dark-state recovery. Although this translocation is expected to occur in ReaChR, as well, it does not coincide with polarity changes around the ICL1.

However, when azF was introduced into the inner gate (Y110azF), a large difference signal was observed in the nonproteinogenic spectral window upon illumination (cf. Figures 4D and 5A). In the closed-state structures of ChRs, a void exists between the inner and central gate called intracellular cavity 1 (cf. Figure S5), which is expected to be filled with solvent. On the basis of the SASA prediction, native Y110 is only poorly hydrated in the dark state (3.9 Å^2). The pronounced signal amplitude can then be explained by the light-induced breakage of the inner gate bonds followed by invasion of the gate interface by water molecules (Figure 6). In contrast, polarity changes within the extended active site and the extracellular half-channel are rather small as deduced from the small amplitude of the azF signals of K133azF and F142azF (cf. Figure 4D and 5A). For K133azF and F142azF, different FTIR signals were detected under photostationary and single-turnover conditions, respectively, because different photointermediates accumulated and/or were detected depending on the applied illumination frequency. According to homology modeling and SASA computations of the dark state, both native amino acids are linked to interior clefts [extracellular cavity (EC) 1 and 2 (cf. Figure 4A)], so that azF might be exposed to local aqueous clusters at corresponding sites already in the dark. This is supported by the increased hydration level of both sites in comparison with Y110 (SASA of 9.3 Å^2 for K133 and 5.7 Å^2 for F142). Thus, the lower IR signal intensity of these residues is explained by the smaller difference between the hydration levels of azF in the closed and open state (Figure 6).

To study the influence of the inner gate on channel gating, in particular with respect to hydration changes, we combined Y110azF with classical site-directed mutants (E122Q, E123Q, R308H, and R308N). While Y110azF-E122Q caused an enlarged and fast-decaying azF difference signal, it was reduced and decelerated in Y110azF-R308H (cf. Figure 5B). This opposite trend could not be correlated with different channel conductivities though (Figure S4D). The kinetic effects could be explained either by alternative hydrogen bonding interactions of the inner gate in the double mutant or by changed pK_a values of the residual glutamate(s). As the architecture and the composition of the inner gate are not conserved among the three high-resolution structures of ChRs (cf. Figure S5ii), an interpretation on the basis of the determined molecular arrangement is rather vague. Therefore, it seems more reliable to evaluate the different signal amplitudes of $\nu_{as}(N_3)$, which suggest that the hydration level near Y110azF is affected by the inner gate mutations. Even though this assumption is challenged by the similar SASA values of native Y110 in the dark state of all inner gate mutants (Figure S6A-D) implying a less significant effect on the water content near Y110azF, the contradiction could be resolved by homology modeling of the inner gate mutants. It reveals that the interhelical plane spanned by Y110 (H1), E122 (H2), and H174 (H3) is smaller in E122Q (Figure S6B) but larger in R308H (Figure S6D). As a consequence, a smaller amount (E122Q) and a larger amount (R308H) of water molecules are assumed to be present in the gate interface of the dark state as compared with that of the wild type (Figure 6c). This hypothesis is supported by the intensities of the difference band pattern in the amide I region, reflecting light-induced hydration of α-helical segments,[61] which can be correlated with the intensities of the azido difference bands. The intensities of both the amide I and the azido bands are increased in Y110azF-E122Q and reduced in Y110azF-R308H as compared with those of Y110azF (cf. Figure 5C, bottom). This correlation shows that light-induced hydration is largely due to the influx of water into the inner gate region. It appears that a smaller volume inside the gate interface correlates with a faster water in- and extrusion, which is in line with the faster decay kinetics of the FTIR spectrum of Y110azF-E122Q and vice versa for Y110azF-R308H (cf. Figure 5B). Taken together, our results suggest that the inner gate acts as a funnel that controls water influx and efflux by modulating the diameter of the intracellular entry site. Accordingly, the diverse effect of inner gate mutations in ChRs, including alteration of photocurrent size, inactivation, ion selectivity, kinetics, and expression level,[8,9,75] can be attributed to altered pore dimensions with capacities for different volumes of water that vary between ChR variants depending on the inner gate configurations.

Surprisingly, the FTIR difference spectrum of Y110azF-E123Q lacks any azido signal around 2100 cm^{-1} (cf. Figure 5B, turquoise, left), while the remaining spectrum resembles that of the azF single mutant; neither UV−vis spectroscopy, electrophysiology (cf. Figure S4), nor homology modeling revealed significant deviations (cf. Figure S6C). This

DOI: 10.1021/acs.biochem.8b01211
Biochemistry 2019, 58, 1275−1286

observation can be explained by considering three different scenarios. First, the sensor itself interacts with the environment; e.g., azF forms a hydrogen bond by receiving a proton from a neighboring proton donor. In the case of the Y110azF-E123Q double mutant, the amide group of the introduced glutamine could overtake this function as it is in the proximity of the label. A direct interaction could suppress any sensitivity of the IR sensor to conformational and/or polarity changes, resulting in a flat line in the difference spectrum. Second, aryl azides could be potentially reduced under elimination of molecular nitrogen to primary amines by a redox reaction with thiols,[57] so that the frequency of the respective oscillation shifts in the proteinogenic window below 1800 cm^{-1} [$\delta(NH)_{aniline} \leq 1620\ cm^{-1}$].[76] Neutralization of the glutamate may cause a reorientation or displacement of a neighboring cysteine, e.g., C106 (not conserved in *Cr*ChR2) or C119, toward azF, as both side chains are >5 Å distant in the modeled dark-state structure (Figure S7), which renders this inactivation mechanism fairly unlikely. Lastly, the inner gate becomes leaky, and water invades the gate interface already in darkness. As the central gate still maintains a tight barrier between the two water fronts, pore formation and passive ion transport are inhibited in the dark state of the double mutant (Figure 6). A similar situation was observed for C1C2 with a deprotonated E123 homologue within molecular dynamics simulations.[9] In this scenario, the target site (Y110azF) would not experience major alterations of solvation between the dark and illuminated states, so that the transition would be IR-silent in the high-frequency window. A major impact of the mutant seems plausible when considering the modeled wild-type structure where E123 (H2) interacts interhelically with N305 and R308 [both H7 (Figure 4A)] and is further supported by the reduced intensity of the amide I bands indicative of global hydration changes in the respective mutant (Figure 5B).

In summary, we applied stop codon suppression to introduce site-specifically the IR-active and polarity-sensitive amino acid azF within the putative ion pathway of several ChRs. Our one-step, *in vivo* labeling technique allowed for a broad spectrum of targets, including solvent accessible and, more interestingly, (partially) embedded sites, which is advantageous over classical *in vitro* cysteine transformation that is limited to exposed sites. In addition, azF is sterically similar to the proteinogenic tyrosine and, thus, smaller and less invasive in comparison with larger labels used for electron paramagnetic resonance (nitroxides) or fluorescence (fluorescein) measurements. Additionally, the latter suffer from a high degree of translational freedom, rendering discrimination between label and protein movements rather difficult. By means of steady-state and time-resolved vibrational spectroscopy, we tracked global [amide I, $\nu_s(C{=}O)$] and local (hydration) changes [$\nu_{as}(N_3)$] in ReaChR simultaneously and could derive the hydration pattern of selected residues in the dark as well as the conducting state along with the dehydration dynamics of the closing channel. In particular, our data reveal that the inner gate acts as an intracellular entry funnel by restricting water influx and efflux in the gate interface. To the best of our knowledge, this study presents the first report of the successful integration and subsequent spectroscopic analysis of an unnatural IR-active amino acid in the class of microbial rhodopsins. The superior labeling technique in combination with the unprecedented spatial resolution within FTIR measurements renders this methodology highly valuable for the interpretation of complex IR spectra as well as the mechanistic elucidation thereof. In the future, earlier hydration events associated with channel (pre)gating will be resolved using IR methods with faster time resolution such as step-scan or quantum cascade laser excitation.

■ ASSOCIATED CONTENT

Supporting Information

The Supporting Information is available free of charge on the ACS Publications website at DOI: 10.1021/acs.biochem.8b01211.

Experimental section, expression kinetics and yields of wild-type channelrhodopsins and azF mutants (Figure S1), Fourier transform infrared spectra of ReaChR and azF mutants (Figure S2), Fourier transform infrared spectroscopy of free *p*-azido-L-phenylalanine (Figure S3), inner gate mutants of ReaChR with the Y110azF backbone (Figure S4), structural differences in channelrhodopsins (Figure S5), influence of mutations on the inner gate structure and intracellular cavity 1 in ReaChR (Figure S6), and cysteines in ReaChR (Figure S7) (PDF)

Accession Codes

C1C2, Protein Data Bank entry 3ug9; *Co*ChR, GenBank entry KF992041; *Cr*ChR2, GenBank entry AF461397; Chronos, GenBank entry KF992040; ReaChR, GenBank entry KF448069; Chrimson, GenBank entry KF992060.

■ AUTHOR INFORMATION

Corresponding Author

*Phone: +49-30-2093-8830. Fax: +49-30-2093-8520. E-mail: Hegemann@rz.hu-berlin.de.

ORCID

Peter Hegemann: 0000-0003-3589-6452

Author Contributions

B.S.K. expressed and purified proteins, performed UV−vis spectroscopy, bioorthogonal labeling experiments, and bioinformatic predictions, and recorded microscopic images. J.C.D.K. performed steady-state FTIR and J.K. rapid-scan FTIR measurements. J.V. conducted and analyzed electrophysiological recordings. T.H. and T.P.S. provided material and experimental expertise. All authors participated in the design of experiments and interpretation of the results. B.S.K. and P.H. wrote the manuscript with further contributions from all authors.

Funding

This work was supported by the German Research Foundation via SFB1078, Projects B2 (P.H.) and B5 (F.J.B.), and the Cluster of Excellence 314 "Unifying Concepts in Catalysis" (Project E4/D4 to P.H.). P.H. is Hertie Senior Professor for Neuroscience and supported by the Hertie-Foundation. T.H. and T.P.S. are supported by The Danica Foundation and an International Research Alliance at the Novo Nordisk Foundation Center for Basic Metabolic Research through an unconditional grant from the Novo Nordisk Foundation to the University of Copenhagen.

Notes

The authors declare no competing financial interest.

■ ACKNOWLEDGMENTS

The authors thank Christina Schnick, He Tian, Manija Kazmi, Maila Reh, Altina Klein, and Thomas Korte for technical

assistance, Eglof Ritter for preliminary measurements, and Christiane Grimm for fruitful discussions. Furthermore, the authors highly appreciate constructive comments from Steven G. Boxer and Peter Hildebrandt.

■ ABBREVIATIONS

aaRS, aminoacyl tRNA synthetase; azF, *p*-azido-L-phenylalanine; ChR, channelrhodopsin; *Co*ChR, *Chloromonas oogama* ChR; *Cr*ChR1, *Chlamydomonas reinhardtii* ChR1; *Cr*ChR2, *C. reinhardtii* ChR2; C1C2, chimera of *Cr*ChR1 and *Cr*ChR2; DDM, *n*-dodecyl *β*-D-maltopyranoside; DIBO, dibenzyl cyclooctyne; DPBS, Dulbecco's phosphate-buffered saline; EC, extracellular side; FTIR, Fourier transform infrared; H, transmembrane helix; IC, intracellular side; ICL1, intracellular loop 1; LED, light-emitting diode; ReaChR, red-activatable channelrhodopsin; RSB, retinal Schiff base; SASA, solvent accessible surface area; SILAC, stable isotopic labeling of amino acids in cell culture; SPAAC, strain-promoted alkyne−azide cycloaddition; SPI, selective pressure incorporation; UV−vis, ultraviolet−visible; wt, wild type.

■ REFERENCES

(1) Zhang, F., Vierock, J., Yizhar, O., Fenno, L. E., Tsunoda, S., Kianianmomeni, A., Prigge, M., Berndt, A., Cushman, J., Polle, J., Magnuson, J., Hegemann, P., and Deisseroth, K. (2011) The microbial opsin family of optogenetic tools. *Cell 147*, 1446−1457.

(2) Vierock, J., Grimm, C., Nitzan, N., and Hegemann, P. (2017) Molecular determinants of proton selectivity and gating in the red-light activated channelrhodopsin Chrimson. *Sci. Rep. 7*, 9928.

(3) Nagel, G., Ollig, D., Fuhrmann, M., Kateriya, S., Musti, A. M., Bamberg, E., and Hegemann, P. (2002) Channelrhodopsin-1: A Light-Gated Proton Channel in Green Algae. *Science 296*, 2395−2398.

(4) Nagel, G., Szellas, T., Huhn, W., Kateriya, S., Adeishvili, N., Berthold, P., Ollig, D., Hegemann, P., and Bamberg, E. (2003) Channelrhodopsin-2, a directly light-gated cation-selective membrane channel. *Proc. Natl. Acad. Sci. U. S. A. 100*, 13940−13945.

(5) Govorunova, E. G., Sineshchekov, O. A., Janz, R., Liu, X., and Spudich, J. L. (2015) Natural light-gated anion channels: A family of microbial rhodopsins for advanced optogenetics. *Science 349*, 647−650.

(6) Wietek, J., Broser, M., Krause, B. S., and Hegemann, P. (2016) Identification of a Natural Green Light Absorbing Chloride Conducting Channelrhodopsin from *Proteomonas sulcata*. *J. Biol. Chem. 291*, 4121−4127.

(7) Kato, H. E., Zhang, F., Yizhar, O., Ramakrishnan, C., Nishizawa, T., Hirata, K., Ito, J., Aita, Y., Tsukazaki, T., Hayashi, S., Hegemann, P., Maturana, A. D., Ishitani, R., Deisseroth, K., and Nureki, O. (2012) Crystal structure of the channelrhodopsin light-gated cation channel. *Nature 482*, 369−374.

(8) Watanabe, H. C., Welke, K., Sindhikara, D. J., Hegemann, P., and Elstner, M. (2013) Towards an Understanding of Channelrhodopsin Function: Simulations Lead to Novel Insights of the Channel Mechanism. *J. Mol. Biol. 425*, 1795−1814.

(9) Takemoto, M., Kato, H. E., Koyama, M., Ito, J., Kamiya, M., Hayashi, S., Maturana, A. D., Deisseroth, K., Ishitani, R., and Nureki, O. (2015) Molecular Dynamics of Channelrhodopsin at the Early Stages of Channel Opening. *PLoS One 10*, No. e0131094.

(10) Kuhne, J., Eisenhauer, K., Ritter, E., Hegemann, P., Gerwert, K., and Bartl, F. (2015) Early Formation of the Ion-Conducting Pore in Channelrhodopsin-2. *Angew. Chem., Int. Ed. 54*, 4953−4957.

(11) VanGordon, M. R., Gyawali, G., Rick, S. W., and Rempe, S. B. (2017) Atomistic Study of Intramolecular Interactions in the Closed-State Channelrhodopsin Chimera, C1C2. *Biophys. J. 112*, 943−952.

(12) Ardevol, A., and Hummer, G. (2018) Retinal isomerization and water-pore formation in channelrhodopsin-2. *Proc. Natl. Acad. Sci. U. S. A. 115*, 3557.

(13) Sattig, T., Rickert, C., Bamberg, E., Steinhoff, H.-J., and Bamann, C. (2013) Light-Induced Movement of the Transmembrane Helix B in Channelrhodopsin-2. *Angew. Chem., Int. Ed. 52*, 9705−9708.

(14) Krause, N., Engelhard, C., Heberle, J., Schlesinger, R., and Bittl, R. (2013) Structural differences between the closed and open states of channelrhodopsin 2 as observed by EPR spectroscopy. *FEBS Lett. 587*, 3309−3313.

(15) Müller, M., Bamann, C., Bamberg, E., and Kühlbrandt, W. (2015) Light-Induced Helix Movements in Channelrhodopsin-2. *J. Mol. Biol. 427*, 341−349.

(16) Siebert, F., Mäntele, W., and Gerwert, K. (1983) Fourier-transform infrared spectroscopy applied to rhodopsin. *Eur. J. Biochem. 136*, 119−127.

(17) Rothschild, K. J., Cantore, W. A., and Marrero, H. (1983) Fourier transform infrared difference spectra of intermediates in rhodopsin bleaching. *Science 219*, 1333−1335.

(18) Siebert, F., and Mäntele, W. (1983) Investigation of the Primary Photochemistry of Bacteriorhodopsin by Low Temperature Fourier Transform Infrared Spectroscopy. *Eur. J. Biochem. 130*, 565.

(19) Barth, A. (2007) Infrared spectroscopy of proteins. *Biochim. Biophys. Acta, Bioenerg. 1767*, 1073−1101.

(20) Siebert, F. (1995) Application of FTIR Spectroscopy to the Investigation of Dark Structures and Photoreactions of Visual Pigments. *Isr. J. Chem. 35*, 309−323.

(21) Engelhard, M., Gerwert, K., Hess, B., Kreutz, W., and Siebert, F. (1985) Light-Driven Protonation Changes of Internal Aspartic Acids of Bacteriorhodopsin: An Investigation by Static and Time-Resolved Infrared Difference Spectroscopy Using [4-^{13}C]Aspartic Acid Labeled Purple Membrane. *Biochemistry 24*, 400−407.

(22) Hauser, K., Engelhard, M., Friedman, N., Sheves, M., and Siebert, F. (2002) Interpretation of Amide I Difference Bands Observed during Protein Reactions Using Site-Directed Isotopically Labeled Bacteriorhodopsin as a Model System. *J. Phys. Chem. A 106*, 3553−3559.

(23) Ong, S.-E., Blagoev, B., Kratchmarova, I., Kristensen, D. B., Steen, H., Pandey, A., and Mann, M. (2002) Stable Isotope Labeling by Amino Acids in Cell Culture, SILAC, as a Simple and Accurate Approach to Expression Proteomics. *Mol. Cell. Proteomics 1*, 376−386.

(24) Gu, S., Pan, S., Bradbury, E. M., and Chen, X. (2003) Precise Peptide Sequencing and Protein Quantification in the Human Proteome Through In Vivo Lysine-Specific Mass Tagging. *J. Am. Soc. Mass Spectrom. 14*, 1−7.

(25) Ong, S.-E., Mittler, G., and Mann, M. (2004) Identifying and quantifying *in vivo* methylation sites by heavy methyl SILAC. *Nat. Methods 1*, 119−126.

(26) Park, K.-S., Mohapatra, D. P., Misonou, H., and Trimmer, J. S. (2006) Graded Regulation of the Kv2.1 Potassium Channel by Variable Phosphorylation. *Science 313*, 976−979.

(27) Gerwert, K., and Siebert, F. (1986) Evidence for light-induced 13-*cis*14-s-*cis* iomerization in bacteriorhodopsin obtained by FTIR difference spectroscopy using isotopically labelled retinals. *EMBO J. 5*, 805−811.

(28) Oh, K.-I., Lee, J.-H., Joo, C., Han, H., and Cho, M. (2008) *ß*-Azidoalanine as an IR Probe: Application to Amyloid Aß(16−22) Aggregation. *J. Phys. Chem. B 112*, 10352−10357.

(29) Ye, S., Huber, T., Vogel, R., and Sakmar, T. P. (2009) FTIR analysis of GPCR activation using azido probes. *Nat. Chem. Biol. 5*, 397−399.

(30) Ye, S., Zaitseva, E., Caltabiano, G., Schertler, G. F. X., Sakmar, T. P., Deupi, X., and Vogel, R. (2010) Tracking G-protein-coupled receptor activation using genetically encoded infrared probes. *Nature 464*, 1386−1389.

(31) Getahun, Z., Huang, C.-Y., Wang, T., De León, B., DeGrado, W. F., and Gai, F. (2003) Using Nitrile-Derivatized Amino Acids as Infrared Probes of Local Environment. *J. Am. Chem. Soc. 125*, 405−411.

DOI: 10.1021/acs.biochem.8b01211
Biochemistry 2019, 58, 1275−1286

(32) Schultz, K. C., Supekova, L., Ryu, Y., Xie, J., Perera, R., and Schultz, P. G. (2006) A Genetically Encoded Infrared Probe. *J. Am. Chem. Soc. 128*, 13984−13985.
(33) Jo, H., Culik, R. M., Korendovych, I. V., DeGrado, W. F., and Gai, F. (2010) Selective Incorporation of Nitrile-Based Infrared Probes into Proteins via Cysteine Alkylation. *Biochemistry 49*, 10354−10356.
(34) Fafarman, A. T., Webb, L. J., Chuang, J. I., and Boxer, S. G. (2006) Site-Specific Conversion of Cysteine Thiols into Thiocyanate Creates an IR Probe for Electric Fields in Proteins. *J. Am. Chem. Soc. 128*, 13356−13357.
(35) Mohrmann, H., Kube, I., Lórenz-Fonfría, V. A., Engelhard, M., and Heberle, J. (2016) Transient Conformational Changes of Sensory Rhodopsin II Investigated by Vibrational Stark Effect Probes. *J. Phys. Chem. B 120*, 4383−4387.
(36) Suydam, I. T., and Boxer, S. G. (2003) Vibrational Stark Effects Calibrate the Sensitivity of Vibrational Probes for Electric Fields in Proteins. *Biochemistry 42*, 12050−12055.
(37) Nydegger, M. W., Dutta, S., and Cheatum, C. M. (2010) Two-dimensional infrared study of 3-azidopyridine as a potential spectroscopic reporter of protonation state. *J. Chem. Phys. 133*, 134506.
(38) Suydam, I. T., Snow, C. D., Pande, V. S., and Boxer, S. G. (2006) Electric Fields at the Active Site of an Enzyme: Direct Comparison of Experiment with Theory. *Science 313*, 200−204.
(39) Choi, J. H., Raleigh, D. P., and Cho, M. (2011) Azido Homoalanine is a Useful Infrared Probe for Monitoring Local Electrostatistics and Side-Chain Solvation in Proteins. *J. Phys. Chem. Lett. 2*, 2158−2162.
(40) Wolfshorndl, M. P., Baskin, R., Dhawan, I., and Londergan, C. H. (2012) Covalently Bound Azido Groups Are Very Specific Water Sensors, Even in Hydrogen-Bonding Environments. *J. Phys. Chem. B 116*, 1172−1179.
(41) Kiick, K. L., Saxon, E., Tirrell, D. A., and Bertozzi, C. R. (2002) Incorporation of azides into recombinant proteins for chemoselective modification by the Staudinger ligation. *Proc. Natl. Acad. Sci. U. S. A. 99*, 19−24.
(42) Dieterich, D. C., Link, A. J., Graumann, J., Tirrell, D. A., and Schuman, E. M. (2006) Selective identification of newly synthesized proteins in mammalian cells using bioorthogonal noncanonical amino acid tagging (BONCAT). *Proc. Natl. Acad. Sci. U. S. A. 103*, 9482−9487.
(43) Tanrikulu, I. C., Schmitt, E., Mechulam, Y., Goddard, W. A., and Tirrell, D. A. (2009) Discovery of *Escherichia coli* methionyl-tRNA synthetase mutants for efficient labeling of proteins with azidonorleucine in vivo. *Proc. Natl. Acad. Sci. U. S. A. 106*, 15285−15290.
(44) Krause, N. (2016) Structural rearrangements upon opening of Channelrhodopsin-2. Doctoral Dissertation. Freie Universität Berlin, Berlin.
(45) Berthold, P., Tsunoda, S. P., Ernst, O. P., Mages, W., Gradmann, D., and Hegemann, P. (2008) Channelrhodopsin-1 Initiates Phototaxis and Photophobic Responses in *Chlamydomonas* by Immediate Light-Induced Depolarization. *Plant Cell 20*, 1665−1677.
(46) Doi, S., Mori, A., Tsukamoto, T., Reissig, L., Ihara, K., and Sudo, Y. (2015) Structural and functional roles of the N- and C-terminal extended modules in channelrhodopsin-1. *Photochem. Photobiol. Sci. 14*, 1628−1636.
(47) Lee, K. A., Lee, S.-S., Kim, S. Y., Choi, A. R., Lee, J.-H., and Jung, K.-H. (2015) Mistic-fused expression of algal rhodopsins in *Escherichia coli* and its photochemical properties. *Biochim. Biophys. Acta, Gen. Subj. 1850*, 1694−1703.
(48) Doi, S., Tsukamoto, T., Yoshizawa, S., and Sudo, Y. (2017) An inhibitory role of Arg-84 in anion channelrhodopsin-2 expressed in *Escherichia coli*. *Sci. Rep. 7*, 41879.
(49) Lin, J. Y., Knutsen, P. M., Muller, A., Kleinfeld, D., and Tsien, R. Y. (2013) ReaChR: a red-shifted variant of channelrhodopsin enables deep transcranial optogenetic excitation. *Nat. Neurosci. 16*, 1499−1508.
(50) Krause, B. S., Grimm, C., Kaufmann, J. C. D., Schneider, F., Sakmar, T. P., Bartl, F. J., and Hegemann, P. (2017) Complex Photochemistry within the Green-Absorbing Channelrhodopsin ReaChR. *Biophys. J. 112*, 1166−1175.
(51) Kaufmann, J. C. D., Krause, B. S., Grimm, C., Ritter, E., Hegemann, P., and Bartl, F. J. (2017) Proton transfer reactions in the red light-activatable channelrhodopsin variant ReaChR and their relevance for its function. *J. Biol. Chem. 292*, 14205−14216.
(52) Inagaki, H. K., Jung, Y., Hoopfer, E. D., Wong, A. M., Mishra, N., Lin, J. Y., Tsien, R. Y., and Anderson, D. J. (2014) Optogenetic control of *Drosophila* using a red-shifted channelrhodopsin reveals experience-dependent influences on courtship. *Nat. Methods 11*, 325−332.
(53) Klapoetke, N. C., Murata, Y., Kim, S. S., Pulver, S. R., Birdsey-Benson, A., Cho, Y. K., Morimoto, T. K., Chuong, A. S., Carpenter, E. J., Tian, Z., Wang, J., Xie, Y., Yan, Z., Zhang, Y., Chow, B. Y., Surek, B., Melkonian, M., Jayaraman, V., Constantine-Paton, M., Wong, G. K.-S., and Boyden, E. S. (2014) Independent optical excitation of distinct neural populations. *Nat. Methods 11*, 338−46.
(54) Kato, H. E., Kamiya, M., Sugo, S., Ito, J., Taniguchi, R., Orito, A., Hirata, K., Inutsuka, A., Yamanaka, A., Maturana, A. D., Ishitani, R., Sudo, Y., Hayashi, S., and Nureki, O. (2015) Atomistic design of microbial opsin-based blue-shifted optogenetics tools. *Nat. Commun. 6*, 7177.
(55) van Geel, R., Pruijn, G. J. M., van Delft, F. L., and Boelens, W. C. (2012) Preventing Thiol-Yne Addition Improves the Specificity of Strain-Promoted Azide−Alkyne Cycloaddition. *Bioconjugate Chem. 23*, 392−398.
(56) Tian, H., Sakmar, T. P., and Huber, T. (2015) Micelle-Enhanced Bioorthogonal Labeling of Genetically Encoded Azido Groups on the Lipid-Embedded Surface of a GPCR. *ChemBioChem 16*, 1314−1322.
(57) Staros, J. V., Bayley, H., Standring, D. N., and Knowles, J. R. (1978) Reduction of aryl azides by thiols: Implications for the use of photoaffinity reagents. *Biochem. Biophys. Res. Commun. 80*, 568−572.
(58) Dyall, L. K., and Kemp, J. E. (1967) The infrared spectra of aryl azides. *Aust. J. Chem. 20*, 1395−1402.
(59) Lipkin, J. S., Song, R., Fenlon, E. E., and Brewer, S. H. (2011) Modulating Accidental Fermi Resonance: What a Difference a Neutron Makes. *J. Phys. Chem. Lett. 2*, 1672−1676.
(60) Silverman, L. N., Pitzer, M. E., Ankomah, P. O., Boxer, S. G., and Fenlon, E. E. (2007) Vibrational Stark Effect Probes for Nucleic Acids. *J. Phys. Chem. B 111*, 11611−11613.
(61) Lórenz-Fonfría, V. A., Bamann, C., Resler, T., Schlesinger, R., Bamberg, E., and Heberle, J. (2015) Temporal evolution of helix hydration in a light-gated ion channel correlates with ion conductance. *Proc. Natl. Acad. Sci. U. S. A. 112*, E5796−5804.
(62) Tian, H., Sakmar, T. P., and Huber, T. (2013) Site-Specific Labeling of Genetically Encoded Azido Groups for Multicolor, Single-Molecule Fluorescence Imaging of GPCRs. In *Methods in Cell Biology* (Conn, P. M., Ed.) pp 267−303, Elsevier Inc., Amsterdam.
(63) Tian, H., Naganathan, S., Kazmi, M. A., Schwartz, T. W., Sakmar, T. P., and Huber, T. (2014) Bioorthogonal fluorescent labeling of functional G-protein-coupled receptors. *ChemBioChem 15*, 1820−1829.
(64) Naganathan, S., Ye, S., Sakmar, T. P., and Huber, T. (2013) Site-specific epitope tagging of G protein-coupled receptors by bioorthogonal modification of a genetically encoded unnatural amino acid. *Biochemistry 52*, 1028−36.
(65) Chin, J. W., Santoro, S. W., Martin, A. B., King, D. S., Wang, L., and Schultz, P. G. (2002) Addition of *p*-Azido-L-phenylalanine to the Genetic Code of *Escherichia coli*. *J. Am. Chem. Soc. 124*, 9026−9027.
(66) Grunbeck, A., Huber, T., Abrol, R., Trzaskowski, B., Goddard, W. A., and Sakmar, T. P. (2012) Genetically Encoded Photo-cross-linkers Map the Binding Site of an Allosteric Drug on a G Protein-Coupled Receptor. *ACS Chem. Biol. 7*, 967−972.

DOI: 10.1021/acs.biochem.8b01211
Biochemistry 2019, 58, 1275−1286

(67) Zhu, S., Riou, M., Yao, C. A., Carvalho, S., Rodriguez, P. C., Bensaude, O., Paoletti, P., and Ye, S. (2014) Genetically encoding a light switch in an ionotropic glutamate receptor reveals subunit-specific interfaces. *Proc. Natl. Acad. Sci. U. S. A. 111*, 6081−6086.
(68) Rannversson, H., Andersen, J., Sørensen, L., Bang-Andersen, B., Park, M., Huber, T., Sakmar, T. P., and Strømgaard, K. (2016) Genetically encoded photocrosslinkers locate the high-affinity binding site of antidepressant drugs in the human serotonin transporter. *Nat. Commun. 7*, 11261.
(69) Klippenstein, V., Ghisi, V., Wietstruk, M., and Plested, A. J. R. (2014) Photoinactivation of Glutamate Receptors by Genetically Encoded Unnatural Amino Acids. *J. Neurosci. 34*, 980−991.
(70) Volkov, O., Kovalev, K., Polovinkin, V., Borshchevskiy, V., Bamann, C., Astashkin, R., Marin, E., Popov, A., Balandin, T., Willbold, D., Büldt, G., Bamberg, E., and Gordeliy, V. (2017) Structural insights into ion conduction by channelrhodopsin 2. *Science 358*, eaan8862.
(71) Oda, K., Vierock, J., Oishi, S., Rodriguez-Rozada, S., Taniguchi, R., Yamashita, K., Wiegert, J. S., Nishizawa, T., Hegemann, P., and Nureki, O. (2018) Crystal structure of the red light-activated channelrhodopsin Chrimson. *Nat. Commun. 9*, 3949.
(72) Eisenhauer, K., Kuhne, J., Ritter, E., Berndt, A., Wolf, S., Freier, E., Bartl, F., Hegemann, P., and Gerwert, K. (2012) In Channelrhodopsin-2 Glu-90 Is Crucial for Ion Selectivity and Is Deprotonated during the Photocycle. *J. Biol. Chem. 287*, 6904−6911.
(73) Richards, R., and Dempski, R. E. (2017) Adjacent channelrhodopsin-2 residues within transmembranes 2 and 7 regulate cation selectivity and distribution of the two open states. *J. Biol. Chem. 292*, 7314−7326.
(74) Volz, P., Krause, N., Balke, J., Schneider, C., Walter, M., Schneider, F., Schlesinger, R., and Alexiev, U. (2016) Light and pH-induced Changes in Structure and Accessibility of Transmembrane Helix B and Its Immediate Environment in Channelrhodopsin-2. *J. Biol. Chem. 291*, 17382−17393.
(75) Sugiyama, Y., Wang, H., Hikima, T., Sato, M., Kuroda, J., Takahashi, T., Ishizuka, T., and Yawo, H. (2009) Photocurrent attenuation by a single polar-to-nonpolar point mutation of channelrhodopsin-2. *Photochem. Photobiol. Sci. 8*, 328−336.
(76) Richtering, H. (1956) Untersuchungen am *IR*-Spektrum von Anilin. *Z. Phys. Chem. 9*, 393−396.

DOI: 10.1021/acs.biochem.8b01211
Biochemistry 2019, 58, 1275−1286